2007 SAE Aero Design East

Long Beach State University
“A TAILLESS TALE”

Team #218
Open Class

APPENDIX
2006 SAE AERO DESIGN

STATEMENT OF COMPLIANCE
Certification of Qualification

Team Name: A TAILLESS TAIL Team Number: 212

School: CALIFORNIA STATE UNIVERSITY AT LONG BEACH

Faculty Advisor: ERIC R KENDALL

Faculty Advisor E-Mail: eric.r.kendall2@boeing.com

Statement of Compliance

As Faculty Advisor, I certify that the registered team members are enrolled in collegiate courses. This team has designed, constructed and/or modified the radio controlled airplane they will use for the SAE Aero Design 2006 competition, without direct assistance from professional engineers, R/C model experts or pilots, or related professionals.

Eric R Kendall

Signature of Faculty Advisor

Team Captain Information:

Team Captain:	DANIEL A. DOUGHERTY
Captain's E-mail:	dannyboydougherty@yahoo.com
Captain's Phone:	562-453-9472

Note: A copy of this statement needs to be included in your Design Report as page 2 (see 60.1).

Table of Contents

I. Introduction

SAE holds an annual Aero Design competition in which the goal is to produce a flying model capable of lifting the maximum payload up to 55 lbs gross takeoff weight. For the 2007 competition, California State University Long Beach has entered the Open Class with a flying wing design named 'A Tailless Tale'. The technical aspects of the design will be presented in detail, but before we present the technical detail; it would be worthwhile discussing the requirements for the Open Class competition that informed the design.

The 2007 Open Class rules require that a fixed wing aircraft may not weight more than 55 lbs including payload and fuel. There are no restrictions on payload size and shape. A maximum of two 0.61 cubic inch gasoline engines may be used in which gearboxes and non-standard fuel may be used to provide enhanced performance. The flight score is given by the following equation:

Flight Score = Raw Weight Score + Prediction Bonus + Zero Payload Bonus + Stopping Bonus

Where: Raw Weight Score = Weight lifted in lbs x 3

Prediction Bonus = 20 – (predicted payload – actual payload)^2

Zero Payload Bonus = 20 points for flight with zero payload

Stopping Bonus = 20% x Raw Weight Score for stopping within landing zone

The aircraft must takeoff within 100 ft and complete one 360-degree circuit of the flying field. The aircraft must then land within a 400 ft landing zone. In addition to the flight score, the total team score includes a written report and an oral presentation. It should be noted that, unless otherwise specified, all calculations are performed at the takeoff condition as this is often the critical condition for aircraft performance.

II. Configuration Selection

Once the requirements for the competition were thoroughly understood, the team analyzed various configurations to determine the one that could best meet the mission requirements. In order to quickly determine the relative advantages and disadvantages of various configurations, the configurations were placed in a matrix and scored based on various Figures of merit (FOM's). The figures of merit were as

follows: 1) Ease of Construction, 2) Cost, 3) Empty Weight, 4) Handling Qualities, and 5) Empirical Data Available. Each FOM was weighted with percentage importance and scored from 1 to 5. The matrix is presented below in Figure 1.

FOM	Weight	Conventional	Bi-Plane	Flying wing	Canard	Theoretical Ideal
Ease of Construction	0.80	3	2.5	3.5	2.5	5
Cost	0.40	3	2.5	3	3	5
Empty Weight	0.90	2.5	2	4	2	5
Handling Qualities	0.90	4	3.5	3.5	3	5
Historical Data	0.60	4	3.5	3	3	5
Total		**11.85**	**10.05**	**12.55**	**9.5**	**18**

Figure 1 – Configuration Scoring Matrix

Of course, the FOM scores and weightings are arguable and depend to a large extent with the team member's familiarity with the particular configuration type. Once the scores were tabulated it was seen that the flying wing design was at least 6% better than any of the other configurations. The main benefit of the flying wing type is its reduced empty weight due to inherent 'span loading' capability, which reduces the maximum spar bending moment and thus structural weight. Another benefit is the ease of construction due to an inherently lower part count; there are no fuselage or tail surfaces to attach since the wing alone houses the payload while providing stability and control. The primary risks with the type are scarcity of historical data and handling qualities. Both of these risks were deemed acceptable since the team was familiar with the flying wing type having both design and flying experience. It should be noted that a flying wing is a highly integrated design, each of the disciplines – aero, stability and control, structures, etc – are coupled to a larger extent than a conventional aircraft. Because of this, the reader will find mention of many other disciplines in each design section since a good flying wing design demands attention across all disciplines before a decision can be reached regarding a particular feature.

III. Planform Selection

Before aerodynamic, stability and control, or structural analysis can be carried out, an initial planform must be selected and then iterated upon through the various design disciplines. A self-imposed

span requirement of 12 feet was chosen – mainly driven by transport, stowage, cost and build schedule concerns.

The planform area was then determined based on an assumed C_{lmax} of 1.0, which is a reasonable assumption given historical data on flying wings (reference 1, page 423). In reference 2, page 10, the calculated mean acceleration was 9.72 ft/sec^2. For our model, it was assumed that the mean acceleration on takeoff ground roll was 8 ft/sec^2. This number was calculated assuming similar static thrust and ground roll drag as the subject aircraft, but changing the weight from 45 lbs to 55 lbs such that 9.72 ft/sec^2 * (45/55) = 8 ft/sec^2. The takeoff speed was calculated using the equation (1):

$$V_{TO} = \text{sqrt}(2\, a_{mean}\, S_g) = 21 \text{ kts} \qquad (1)$$

Where: Sg = 75 ft takeoff distance (100 ft * 75% - T.O. margin)

S_{ref} was then calculated to be 5300 in^2 using the equation for C_{lmax} to solve for Sref:

$$C_{lmax} = W / (1/2\rho V^2 * S_{ref}) \qquad (2)$$

Given: W = 55 lbs
ρ = .00238 lb/sqft
V = 35.5 ft/sec (21 kts)

The aspect ratio was a fallout of the span and planform area, where AR = span^2/Sref = 3.9.

Now that the team had calculated an initial planform area, span, and AR; it was time to choose the leading edge sweep (LE sweep). A survey of existing swept flying wing models and previous production flying wings such as the B2 and B49 show the LE sweep to vary from 18 deg for competitive sailplanes such as the CO5 to 33 deg for the B2. When comparing various LE sweeps, one parameter used was the effective 'tail length' due to sweep. This is given by (reference 1, page 420):

$$\text{Flying Wing Tail Length} = .5\ (\text{span}) * \tan(\text{LE sweep}) \qquad (3)$$

An increase in tail length will benefit two key areas: 1) increase the longitudinal control power of the elevons and 2) facilitate a larger CG envelope. However, increased sweep decreases C_{lmax} and increases span wise flow which causes tip stall. Therefore, a LE of 25 degrees (an average of the surveyed flying wings) was chosen as a good balance between stability and control and performance.

The leading edge now designed, the team focused on the trailing edge of the planform. It was laid out such that there was an aft extension in the middle portion of the wing. This served the dual purpose of 1) moving the aerodynamic center of the planform aft, thus allowing easier packaging of payload, and 2) allowing an effective longitudinal pitch control surface since it is relatively far aft of the CG. The outer wing panels were then designed as un-tapered sections to facilitate ease of construction. The resulting planform is shown in Section X.

IV. Aerodynamics

Once the planform was designed, an airfoil needed to be selected and analyzed. The main requirements of the airfoil were high C_{lmax}, gentle stall and neutral to positive (nose up) pitching moment. The first two items, high C_{lmax} and gentle stall are desirable regardless of configuration, however a neutral to positive pitching moment airfoil is unique to flying wing design. For a statically stable flying wing, trim can be achieved through 1) airfoil 'reflex' (s-shaped camber line with negative camber at the trailing edge), 2) negative trailing edge deflection (TE up), or 3) washout at the wing tips (LE twisted down). Often a combination of these methods is used for longitudinal trim, however there are larger performance penalties for methods 2) and 3). Negative TE deflection is essentially a 'reflexed airfoil', but the surface deflection creates a discontinuous airfoil shape that compares unfavorably in drag. While wing washout greatly reduces the total lifting capability of the wing since the outer wing sections are at a lower angle of attack and thus are producing less lift at a given alpha. This can be understood as an effective decrease in wingspan. For these reasons, a positive pitching moment airfoil was deemed most desirable.

The University of Illinois at Urbana-Champaign aerodynamics website, http://www.ae.uiuc.edu/m-selig/ads/coord_database.html, was used to survey the existing flying wing airfoils. Many airfoils were downloaded and analyzed in XFLR5, a publicly available airfoil analysis program that provides fully viscous 2D section analysis and vortex lattice method analysis for 3D effects. The results of some of the airfoils analyzed in XFLR5 are shown in Figure 2. The chosen airfoil, MH78, is marked with an arrow.

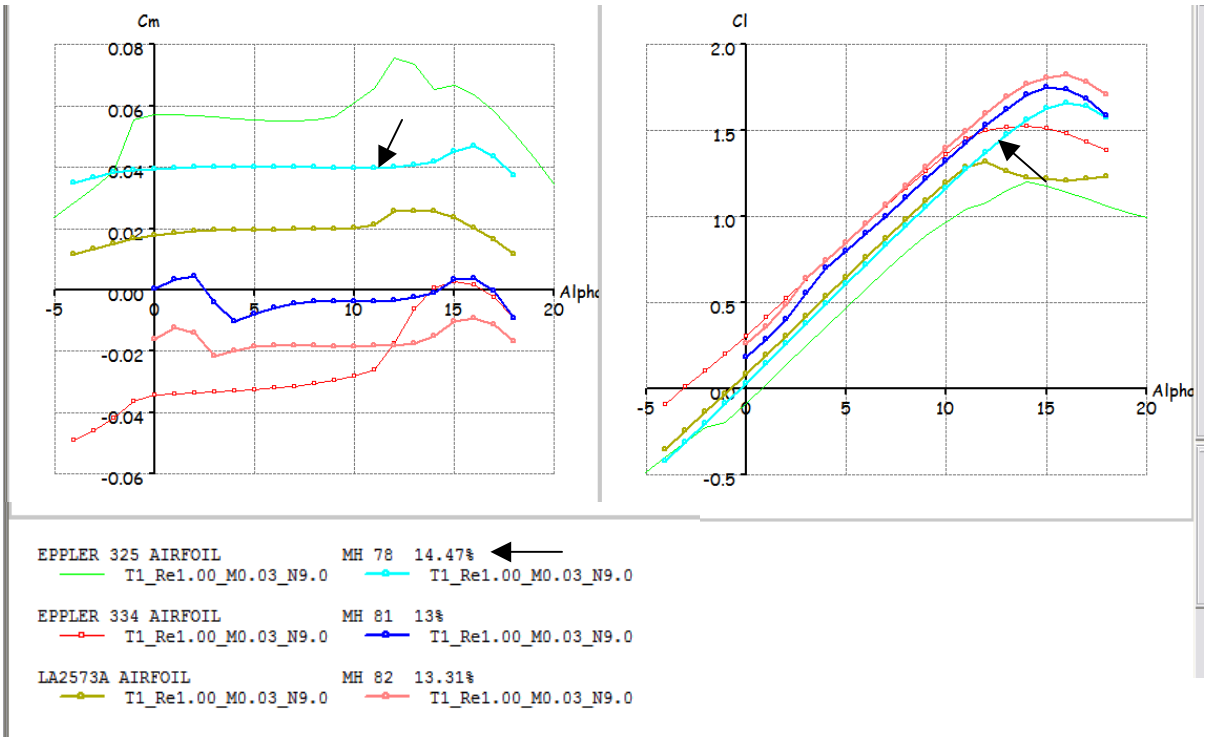

Figure 2 – Airfoil Selection

As can be seen, MH82 has the highest C_{lmax} of 1.8. However, it has the second largest negative pitching moment, $C_{m\alpha}$ = -0.02. MH78 has a C_{lmax} of 1.65, which is within 8% of MH82, and a $C_{m\alpha}$ = 0.04. Also, MH78 has a t/c of 14.7%, which will be useful in packaging payload and reducing structural weight. For these reasons MH78 was chosen. However, in order to attain a higher C_{lmax}; the airfoil was modified by increasing the camber at the trailing edge by 2 degrees at 75% chord. Figure 3 shows the MH78M (modified) vs. the original MH78 section. MH78M has increased max lift by 6% to 1.75, and reduced the pitching moment to 0.02.

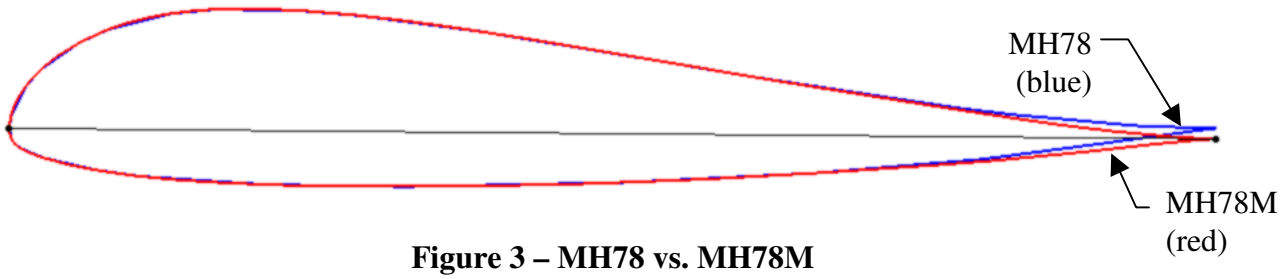

Figure 3 – MH78 vs. MH78M

It should be noted that the MH78 airfoil requires a trip strip at 12.5% chord to reduce the possibility of laminar flow and the attendant instantaneous separation at high AOA.

The airfoil now chosen, two key aerodynamic parameters for the 3D wing were zero lift angle of attack, C_{lo}, and change in lift with change in alpha, $dC_L/d\alpha$. C_{lo} is mostly dependant on airfoil camber. $dC_L/d\alpha$ is essentially linear up to stall and is strongly affected by quarter chord sweep and aspect ratio. Both of these parameters directly determine the lifting performance of the aircraft. The planform points were entered in XFLR5, panel mesh was created, and vortex lattice results calculated at the T.O. speed of 25 kts. These results were compared with the DATCOM equation for $dC_L/d\alpha$:

$$dC_L/d\alpha = 2\pi / [2 + AR^2\beta^2 / k^2(1 + \tan^2\Lambda_{c/2} / \beta^2) + 4)^{1/2} \quad (4)$$

Where: $\beta = (1-M^2)^{1/2}$ (5)

$\Lambda_{c/2}$ = sweep at ½ chord

The results of the comparison are quite good. For the given planform, $C_{L\alpha}$ from DATCOM and XFLR5 is 0.066 and 0.065 respectively. The zero lift AOA was calculated at –1.0 deg per Figure 4.

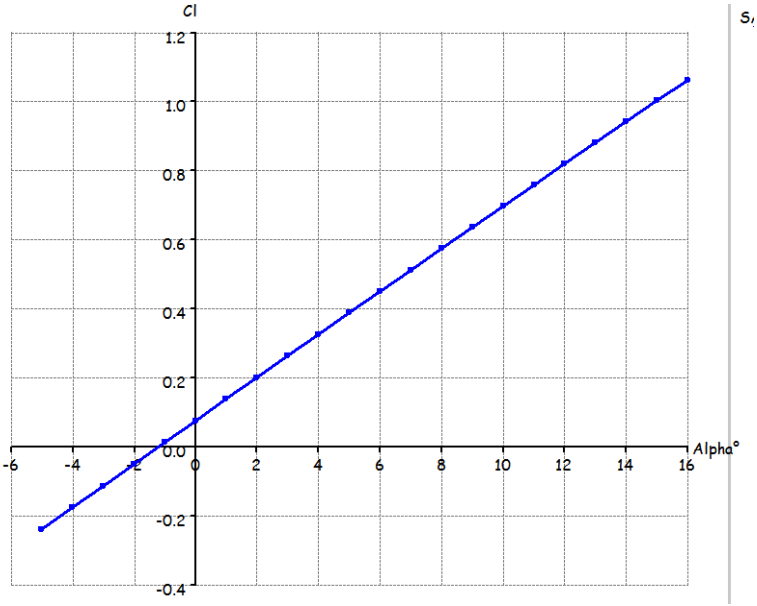

Figure 4 – C_L vs. Alpha for Planform

C_{Lmax} of the planform was calculated using equation (6) from reference 3, page 328:

$$C_{Lmax} = 0.9\, Clmax\ (\cos\Lambda_{.25c}) = 1.36 \quad (6)$$

The addition of slats further increased the C_{Lmax} by 0.15 to 1.51 (reference 3, page 340). This value was multiplied by 0.7 to guard against gusts, over-rotation, and maneuver near the ground. This gave an operational C_{Lmax} of 1.06, which is very close to the original assumption of 1.0. The new takeoff speed was calculated to be 20.5 kts using equation (2).

The next aerodynamics challenge to be tackled was protecting against tip stall. LE sweep, as mentioned in Section III, helps increase longitudinal control and CG envelope. However, increased LE sweep also increases span-wise flow, which can cause tip stall. In order to keep the flow attached over the outer wings, fixed slats were utilized forward of the span section with elevons (see Section X). In this way, the center section will stall first, creating a nose down pitching moment. Meanwhile, due to slats, the outer elevons are operating in fully attached flow, allowing full pitch control through the stall. This effect is confirmed in reference 1, page 423. Slat shape and placement were roughly based on the successful PZL-104 Wilga design per reference 4, page 1.

Lastly, it was decided that winglets would be added to the wing tips. These provided increased yaw stability and control and increased the effective span. Based on empirical data, the addition of winglets increases the aspect ratio by roughly 20% from AR4 to AR5 (reference 3, page 324). This directly increases the lifting capability of the aircraft by increasing the slope of the $C_{L\alpha}$ curve from .065 to .071.

V. Stability and Control

Static longitudinal stability, dC_m/dC_L, is the change in pitching moment vs. change in lift coefficient. In order for an aircraft to be statically stable, the slope of this curve should be negative such that the aircraft pitches nose down with increasing lift coefficient. The team quickly decided that the aircraft would be statically stable in order to achieve good flying qualities and reduce electronics cost and complication. This requires that the 'static margin' (SM) must be positive, or, put another way, the CG must be forward of the aerodynamic center (AC) .

The equation for static margin is simply:

$$SM = (X_{AC} - X_{CG}) / MAC$$

Where: X_{AC} = x loc. of aerodynamic center
X_{CG} = x loc. of center of gravity
MAC = mean aerodynamic chord = 40.45 inches

The MAC = 40.45 inches and was calculated by summing the area weighted MAC's of each tapered section of the planform.

XFLR5 was used to calculate the AC location on the planform, in order to determine where the CG should be placed for positive SM. The AC was calculated at approximately 24.2% of the MAC, which is in agreement with general theory that holds that the AC is roughly 25% of MAC. Therefore, to remain statically stable, the CG must be forward of X = 23.75 inches, where X=0 is at the LE vertex of the planform (see Section X). In our case, the aircraft must maintain a static margin of no less than 5%, requiring the CG to be forward of X = 21.75 inches. This was determined to be a good compromise between flying qualities and performance since an increased static margin improves stability, but reduces performance due to greater trailing edge deflections required for trim.

It should be noted that the static margin is affected by power as well as CG placement. For tractor layout flying wings, it is recommended that the AC of the wing sections immersed in the slipstream are forward of the CG (reference 1, page 424). Also, it is desirable to have the thrust line going through the CG or be slightly above the CG. Both of these features will produce a stabilizing effect with the addition of power. A destabilizing effect will occur if the AC of the 'immersed' wing sections are forward of the CG. Essentially the entire center section of our planform directly aft of the propellers is immersed in prop wash. The resulting 'immersed' wing has an AR = 0.5, and span = 30 inches.

In order to locate the AC of the immersed planform section, a 20% sheet foam glider was created with AR=0.5, span = 6". The CG was then placed at the 20% MAC location of the full-up planform. Test flights were made and it was seen that the glider was roughly neutrally stable to slightly unstable. This means that power will have a destabilizing effect on the aircraft. Modifying the thrust axis such that it passes above the CG can mitigate this destabilizing effect.

Directional stability, $dCn/d\beta$, is another important factor in the aircrafts' flying qualities. This term can be described as change in yawing moment vs. change in sideslip angle and should have a positive slope for static directional stability. The contribution of the vertical tail to directional stability is given below (reference 5, pg. 78):

$$dC_{nv}/d\beta = V_v \eta_v C_{L\alpha v}(1 + d\sigma/d\beta) \quad (7)$$

Where: V_v (vertical tail volume) $= l_v S_v / Sb = .02117$
$\eta_v = Q_{vertical} / Q_{wing} = 1$
σ = sidewash angle over tail = 1
β = sideslip angle
$C_{L\alpha v}$ = lift slope curve of vertical tail

The lift slope of the vertical tail, $C_{L\alpha v}$, is calculated using equation (4). The first cut at vertical tail geometry assumed a span of 18 inches and an AR of 1.8. This gives a $C_{L\alpha v}$ of 0.0388.

Wing sweep also has a positive effect on static directional stability. This is given by (reference 3, pg 510):

$$dC_{nw}/d\beta = C_L^2 \{ 1/(4\pi AR) - [\tan\Lambda / (\pi AR(AR+4\cos\Lambda))] \quad (8)$$

$$[\cos\Lambda - AR/2 - AR^2/8 \cos\Lambda + 6(X_{ACw}-X_{CG})\sin\Lambda/AR]\}$$

As can be seen, sweep and C_L largely affect wing directional stability such that increasing sweep or C_L will increase wing alone directional stability. An Excel spreadsheet was created to calculate the $dC_n/d\beta$ of the entire aircraft at varying C_L's both at takeoff and cruise conditions. The target for adequate directional static stability was a $dC_n/d\beta > 0.001$/deg (reference 1, pg 428). As seen in Figure 5, $dC_n/d\beta$ is 0.012 at cruise and 0.032 at takeoff. Due to the dihedral effect of sweep, dihedral was deemed unnecessary.

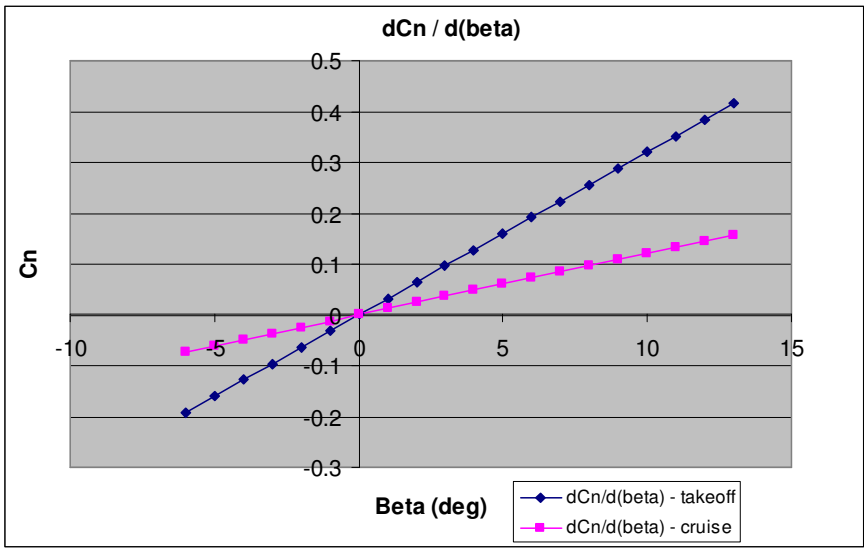

Figure 5 – Directional Stability at Takeoff and Cruise

As a final check for adequate longitudinal and directional stability margin, a test glider of 20% scale (36 inch span) was cut out of foam sheet, and the CG placed at 20% MAC (5% stable) to confirm that the correct AC location had been calculated. The glider had no dihedral, and was a 'flat plate' airfoil section. This glider exhibited excellent longitudinal and directional stability, and provided validation of the theoretical calculations.

Finally, it was necessary to determine whether the aircraft had adequate longitudinal and directional control power. First, longitudinal control power at takeoff was analyzed. XFLR5 was used to calculate the change in pitching moment vs. change in TE deflection, $dC_m/d\eta$. It was also used to calculate change in lift coefficient vs. change in TE deflection, $dC_L/d\eta$. These values are critical in determining the control power and trimmed lift coefficient for the aircraft.

The MH78M airfoil was modeled with 10 deg TE deflection at 75% chord. These airfoils were then laid into the planform and a vortex lattice analysis was conducted comparing change in pitching moment and lift coefficient between the faired and deflected planforms. Per Figure 6, when subtracting the faired case from the deflected case at a given alpha, $dC_M/d\eta = -0.016$ and $dC_L/d\eta = 0.041$. However, the TE flaps only occupy 72.5% of the span, so the corrected $dC_m/d\eta = .725*-0.016 = -0.012$. Likewise, the corrected $dC_L/d\eta = 0.041*.0725 = 0.03$.

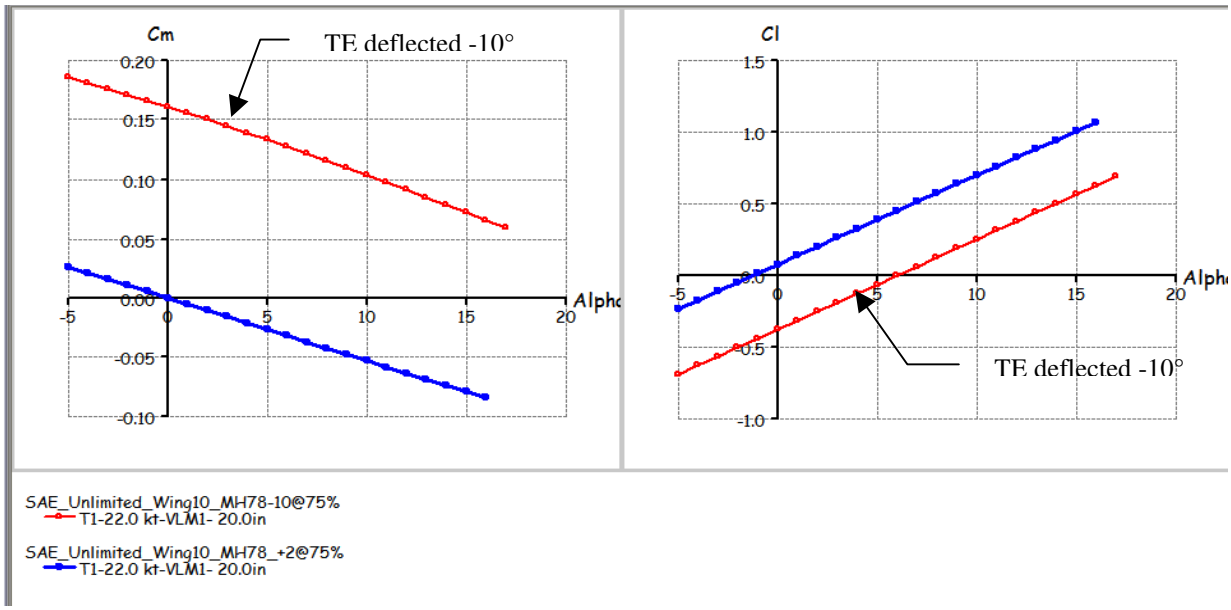

Figure 6 - $dC_m/d\eta$ and $dC_L/d\eta$

The control deflection required for T.O. rotation was determined by equations (9) & (10):

$$\eta_{rotation} = (C_{M0w} + C_{Mcg})/ (dC_m/d\eta) = (0.138+0)/(-.012) = -11.5 \text{ deg} \quad (9)$$

Where: $C_{M0w} = C_M$ of wing at 0 deg AOA = 0 per Figure 6
$C_{Mcg} = C_M$ due to CG location about main landing gear

$$C_{Mcg} = \text{GTOW} * \text{Dist. from CG to Main Gear}/ (q*Sref*MAC) = 0.138 \quad (10)$$

Where: GTOW = 55 lb
Distance from CG to Main Gear = 5.25
q = 1.46 psf
Sref = 5118 sqin
MAC = 40.45 in

This TE deflection is well within the linear range and showed that the initial configuration had the right combination of sweep and control sizing to rotate at 55 lbs Max T.O. weight.

Now that the takeoff rotation was calculated, it was necessary to calculate the up and away flight trim deflections for various CG locations. For this task, the trim deflection for a given C_L was calculated using the following equation (reference 5, pg. 21):

$$d\eta_{trim} = [1/(dC_L/d\eta)] [(C_L *4*(dC_m/dC_L) + C_{L0}] \quad (11)$$

Where: $dC_L/d\eta = 0.03$ (Figure 6)
$4* dC_m/dC_L = 4*-0.05 = -0.2$

Once the trim deflection was known for a given C_L, Equation (12) was used to calculate the trimmed angle of attack:

$$\alpha_{trim} = (C_L + d\eta_{trim} * dC_L/d\eta)/(dCl/d\alpha) \quad (12)$$

Using equations (9) and (10) in an XCEL spreadsheet, $d\eta_{trim}/dC_L$ and α_{trim} were calculated for various static margins and plotted in Figures 7 and 8 respectively.

As can be seen, there is a significant performance penalty to be paid for increasing the static margin. Per Figure 8, a change in static margin from 5% to 10%, decreases $(dCl/d\alpha)_{trim}$ from .0567 to .0427, resulting in a 25% reduction in lift at a given alpha. Meanwhile, Figure 7 shows that the elevator will quickly overshoot the limits of the linear range in order to achieve a $C_L = 1.0$ at a 10% static margin. However, the 5% static margin curve shows the trimmed control deflection is well within the linear

range well beyond $C_L = 1.0$. This further confirmed the design decision to keep a 5% static margin for efficient operational flight while achieving adequate stability.

Takeoff rotation alpha was then calculated by $\alpha_{takeoff} = C_{Ltakeoff} / (dCl/d\alpha)_{trim} = 1.06/.0567 = 18.7$ degrees. This alpha is quite large compared to the 2D section, which stalls around 15 degrees. This is driven by a 20% reduction in $dC_L/d\alpha$ from 0.071 to 0.0567 necessary to trim the 5% static margin. Also, it is due to 3D effects of sweep and low aspect ratio. Both of these factors act to 'unload' the airfoil, allowing it to operate at higher alphas before stalling.

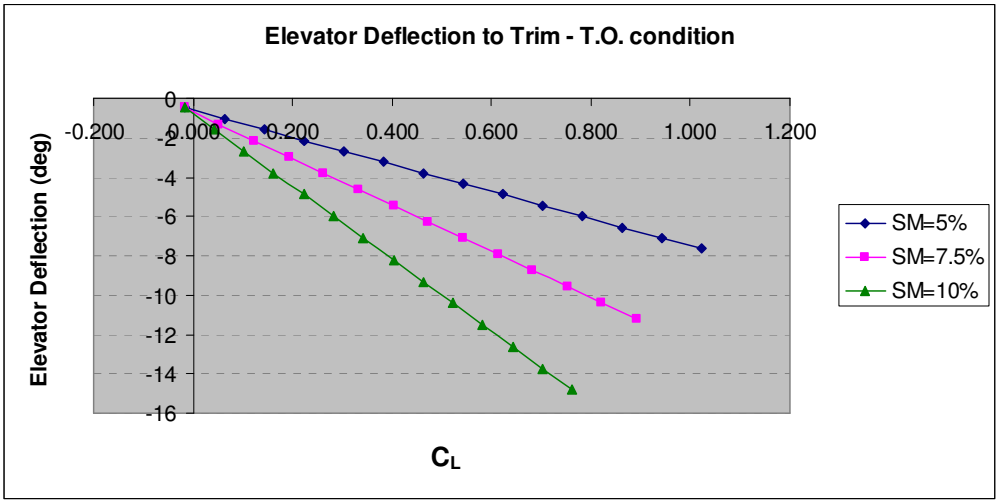

Figure 7 – Elevator Deflection to Trim at T.O. Condition

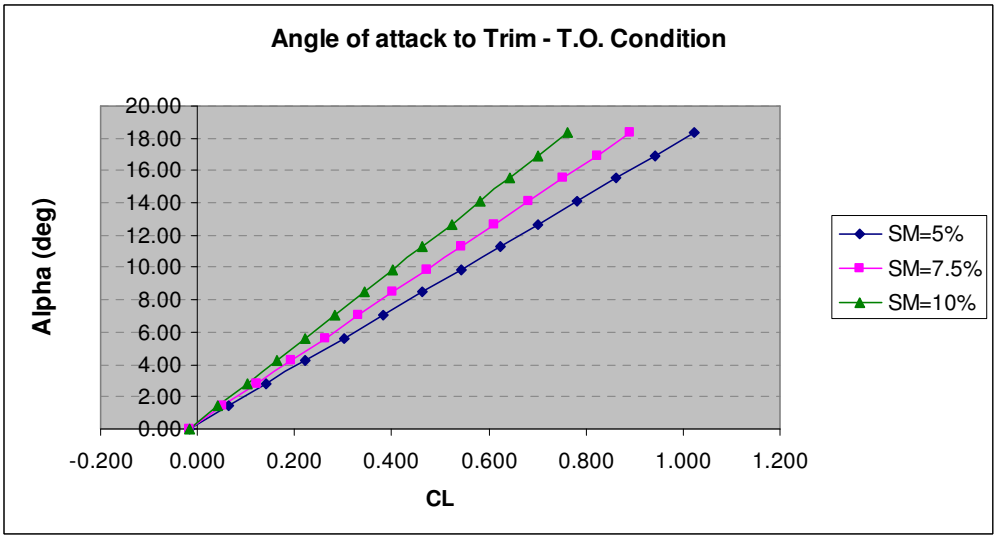

Figure 8 – Angle of Attack to Trim at T.O. Condition

VI. Structures

The structure was laid out such that there was a forward and aft spar. Due to the long chord of the center section and the necessity to remove the torsion inherent in swept wing structure, the structure employs a 2-spar layout. The structure was arranged such that the CG was in between the forward and aft spar, thus providing a very strong box structure to incorporate the payload bays. Outboard of the payload are the engines, and outboard of the engines are the landing gear. See Section X for the structural layout details.

An XCEL spreadsheet was created to calculate the inertial loads, wing air loads, shear diagram and bending moment diagram for the spars. It was assumed that the wing has a roughly elliptical span load, which was confirmed in XFLR5. The inertial loads were calculated based on estimated structures, hardware and payload weights at the given preliminary structural layout locations. The wing load diagram is shown in Figure 9 for a 2G load.

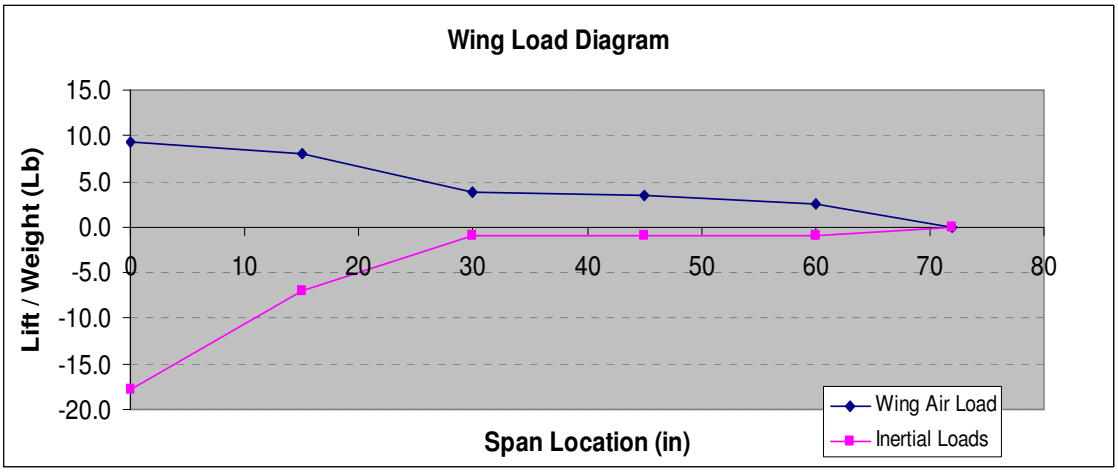

Figure 9 – Wing Loading Diagram

Of note in the wing loading diagram is the span-wise distributed inertial loads from 0 to 30 inches in the payload bay section. Also, due to the increased section chord across the payload section, the wing lift is well located above the inertial loads. This is important in reducing the root bending moment on the spar, thus reducing structural weight.

Next, the shear and bending moment diagrams can be calculated in order. Figure 10 and 11 show the shear and bending moment diagrams for the 2G loads.

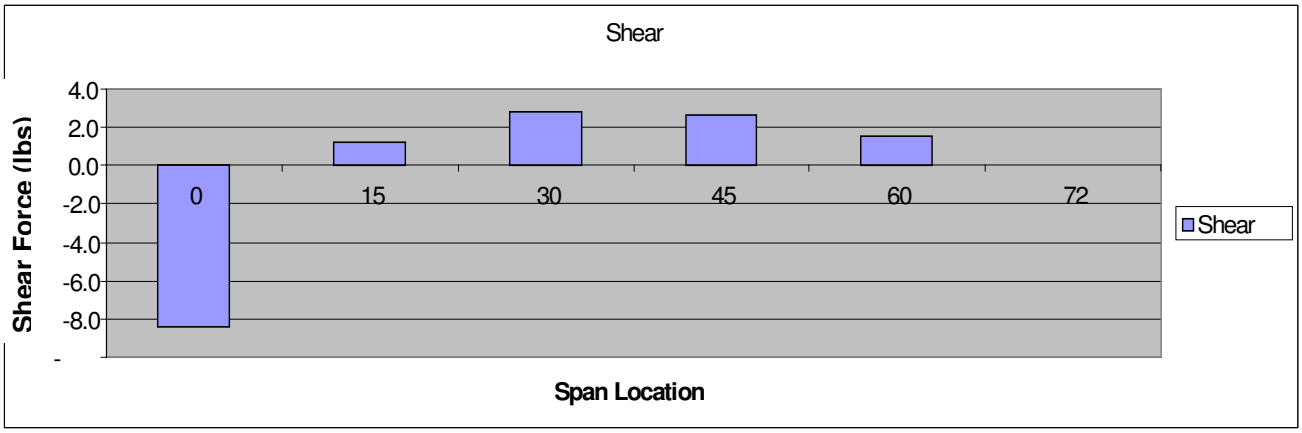

Figure 10 – Shear Diagram

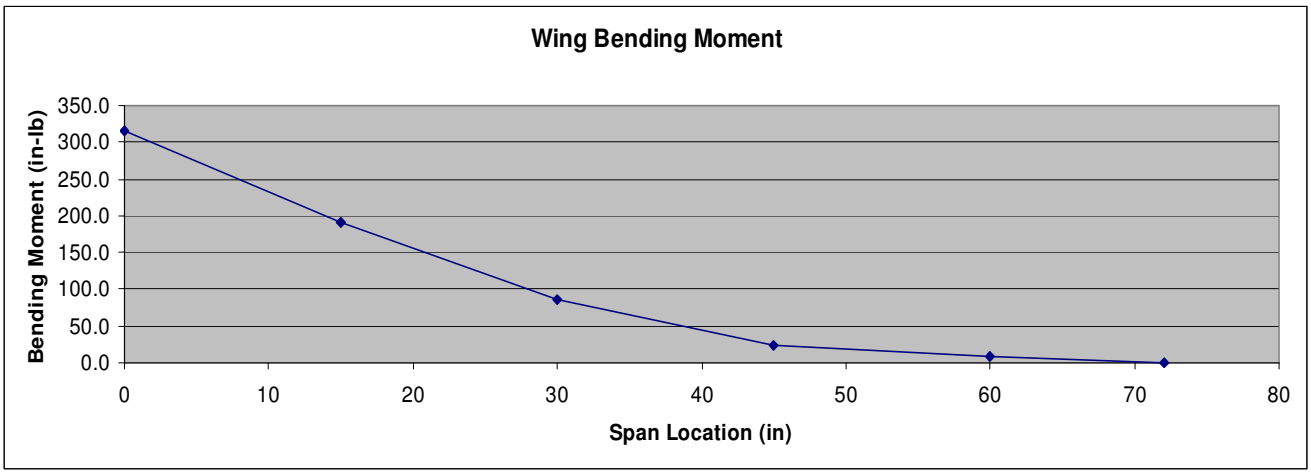

Figure 11 – Wing Bending Moment Diagram

Since the spars are roughly located equidistant from the center of lift, each was sized equally. Based on a conservative section depth of 3.5 inches (the center section is up to 8.8 inches deep), the spars were sized using the following equation:

$$\text{Stress} = (\text{Bending Moment} * \text{Section Depth}/2) / \text{Section Inertia} \quad (13)$$

The ½ inch x ¼ inch spruce spar caps with 1/8 inch balsa shear webs were selected for their ease of construction, excellent strength to weight ratios and low cost. There were plywood shear webs located in the payload, engine and gear bays to form stiffer, more durable structure to attach the various required fittings. As can be seen in Table 12, the spruce spar caps are far from taking the maximum allowable load of 9400 lb/sqin.

Span Location (in)	Section Stress per Spar (psi)
0	584.6
15	355.8
30	315.1
45	85.6
60	34.2
72	0.0

Table 12 – 2G Section Stress

Next to be sized was the landing gear. 1/8" thick, 6061 T6 aluminum plate stock was chosen for its excellent strength to weight ratio and ease of machining. The gear was stressed such that on the worst case landing load, a single main gear takes 2 x 55lbs load. The bending stress was analyzed using the following figure:

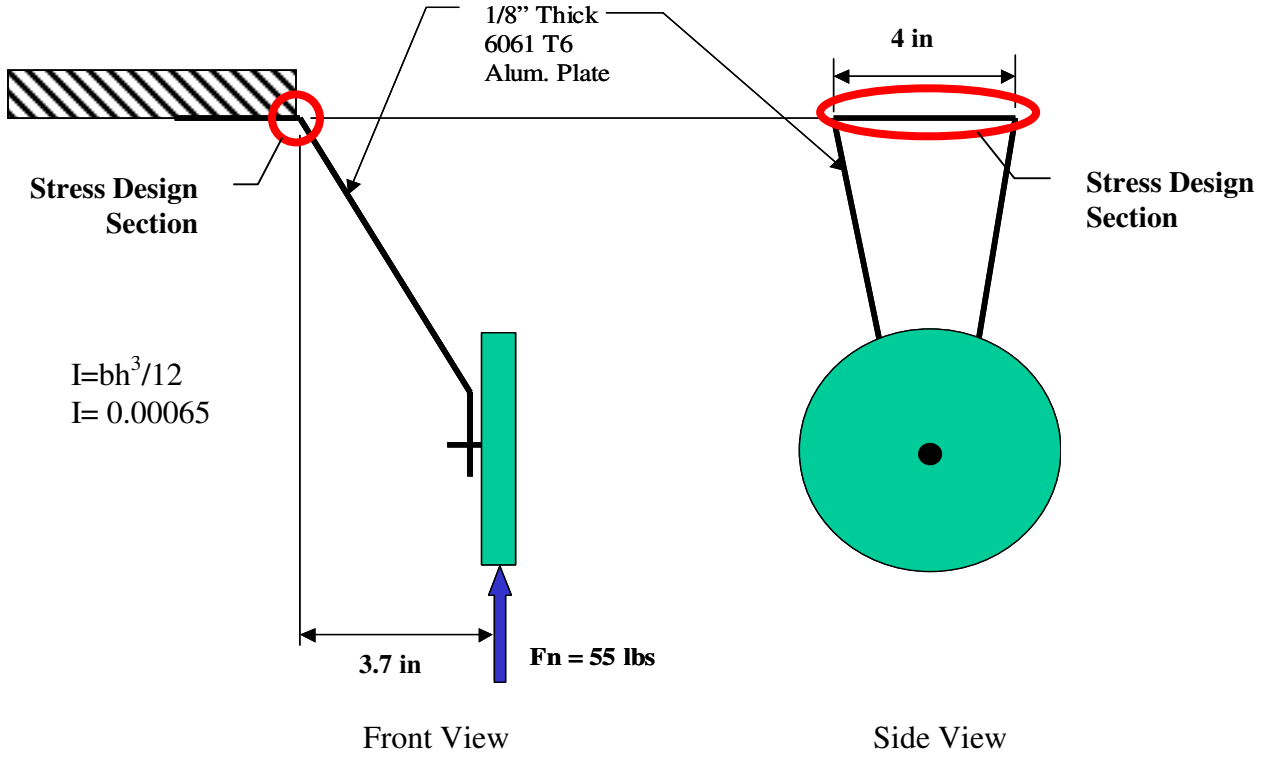

Figure 13 – Main Landing Gear

The stress is concentrated as shown in the red area since this is the clamped portion of the beam, and the gear leg will act like a cantilevered beam.

The gear was found to have a max section stress of:

$$\sigma = MC/I = (3.7in \times 110\ lb \times .125/2)/0.00065 = 39{,}000\ psi.$$

The max allowable stress for 6061T6 is 45,000 psi, so there is a 1.15 safety factor for the worst case 2G condition. Max deflection of the gear was calculated using the cantilevered beam bending equation:

$$\text{Max Deflection} = WL^3/3EI = 0.3 \text{ inches} \qquad (14)$$

Were: E = 1,000,000 lb/sqin
I = 0.00065
L = 3.7 in
W = 110 lbs

Finally, a structural attach method was devised for the outer wing panels. These needed to be removable in order to store and transport the aircraft economically. In order to create a stiff box structure at the wing attach joints, the outboard bays of the center section and inboard bays of the wing panels were reinforced with plywood gussets and shear webs. Then the outer ribs of the center body and wing panels were reinforced with plywood and an aluminum piano hinge was bolted in a vertical orientation between the upper and lower spar caps of the forward and aft spars. In this way, the load is driven primarily to the upper and lower spar caps and the stiffened 'box' sections at the wing joint. The primary concern is pull through load of the bolts through the plywood reinforced ribs, so aluminum plate was used to in-lieu of washers for the nut clamp up to the rib. Also, to ensure minimum mechanical play in the joint, a slightly oversized 1/8" pin was used in the piano hinge.

VII. Propulsion

The rules dictate that no more than two 0.61 engines are allowed on unlimited class aircraft. The team did a survey of the performance of available 0.60 engines using reference 6, and chose the Tower Hobbies .61BB ABC engine. It had the highest brake horsepower of 1.59 at 14,150 RPM and the highest BHP to weight ratio of 1.08. For balance, the engines were arranged in a tractor configuration. They are close to centerline to minimize thrust induced yawing moment due to engine out or asymmetrical thrust.

The static thrust of the engine/propeller combination was found using equation (15), (reference 3, page 396):

$$T_{static} = C_t/C_p[550bhp/(nD)] \quad (15)$$

Where: Ct/Cp is per lookup chart in reference 3
bhp = per test results in reference 6
n = rev/sec, reference 6
D = propeller diameter in ft.

Reference 6 listed test results for bhp, RPM, and torque for various propellers on the Tower Hobbies 0.61 engine. This data was used to in calculating Ct/Cp per reference 3, page 397. It was found that Ct/Cp varies between 1.8 to 3.0 depending on the engine/propeller bhp and RPM. A listing of static thrust for each propeller is given in Table 14:

Prop Dia	Prop Pitch	RPM	Torque (lb-ft)	Static Thrust (lb)
11	6	14450	0.54	10.7
11	7	14150	0.57	11.3
11	8	12850	0.53	10.2
11	11	10950	0.56	7.2
12	6	12150	0.53	9.7
12	7	11250	0.54	9.3
13	7	10450	0.58	9.6
12.5	9	9750	0.55	9.8

Table 14 – Static Thrust

Based on this data, the APC 11x7 propeller was chosen as it had the maximum static thrust of 11.3 lb. Given the static thrust, we were now able to calculate the dynamic thrust. Dynamic thrust decreases linearly with forward airspeed. This relation is also found in reference 3, page 397. Figure 15 shows dynamic thrust vs. airspeed for the APC 11x7 propeller.

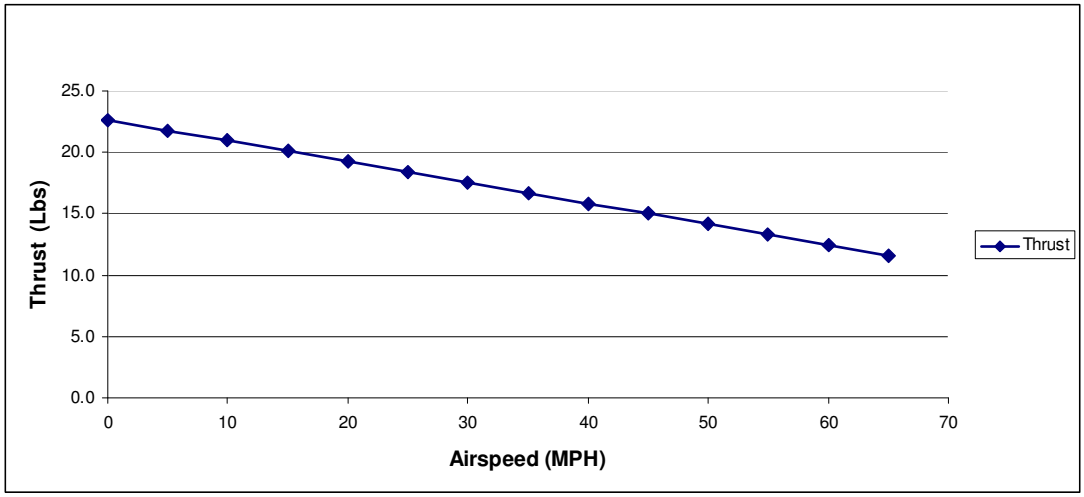

Figure 15 – Dynamic Thrust vs. Airspeed

VIII. Weights and Balance

In order to get an accurate weight and CG location of the aircraft, the team modeled everything in a 3D CAD program. This included assigning densities to all of the structural members, electronics, engines, landing gear, fuel, payload, etc. This took a bit of effort, but since the CG location is so critical on this aircraft, it was felt the effort was warranted.

The empty weight of the aircraft was calculated to be about 25 lbs. This allowed for 30 lbs of payload to be carried for a payload to GTOW ratio of 1.375. Also based on the CAD model, the CG of the aircraft with no payload was found to be at X = 22.05, with a static margin of 4.3%. This is within 1% of the 5% stable requirement. With full payload, the CG moves from X=22.05 to X=21.87, thus the aircraft becomes more stable and is very close to the 5% stable goal. It should be noted that the engines were designed such that they can slide forward and aft within the engine mounting structure. This was done in order to allow fine-tuning of the CG before first flight. An image of the 3D CAD model used to calculate the weights and CG is shown in Figure 16.

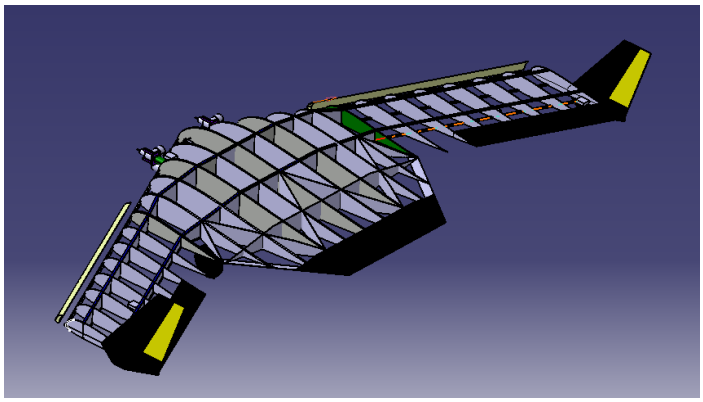

Figure 16 – 3D CAD Model of Configuration

IX. Performance

Once all of the key disciplines had confirmed the validity of the design, a performance analysis was run on the configuration to determine the aircraft closes on the mission requirements. The key performance parameter is takeoff distance with max payload. For this condition, the velocity of the aircraft was assumed to be 21 kts per section I. First, a low speed drag polar was be calculated. The aircraft's drag is the sum of the skin friction drag and the induced drag. Skin friction drag was calculated assuming fully turbulent flow. The equation for skin friction is from reference 3, pg. 342:

$$C_{D0} = \Sigma(C_{fc} FF_c Q_c S_{wetc})/Sref + C_{Dmisc} \qquad (16)$$

Where:
C_{fc} = component flat plate skin friction
FF_c = component form factor
Q_c = component interference effects (neglected)
S_{wetc} = component wetted area
S_{ref} = planform area
C_{dmisc} = miscellaneous items such as flaps, gear, etc.

For turbulent flat plate skin friction, an equation from reference 3, PG 343 was used:

$$C_f = 0.455 / [(\log_{10}Re)^{2.58} (1+0.144M^2)^{0.65}] \qquad (17)$$

Where:
Re = Reynolds number = $\rho vL/\mu$
L= characteristic length

Figure 12.21 in reference 3, PG 321, gives the turbulent C_f based on the Reynolds number.

The component form factor used for the wing and vertical tails was found in reference 3, pg 344:

$$FF = [1 + (0.6/(x/c)_{max})(t/c) + 100(t/c)^4][1.34M^{0.18}(\cos\Lambda_{max})^{0.28}] \quad (18)$$

Where: $(x/c)_{max}$ = chord wise location of the airfoil max thickness
t/c = airfoil thickness/chord
Λ_{max} = sweep of the maximum thickness line

The aircraft components consisted of the wing, vertical tails, landing gear, engines, and flaps. The C_{Do} for flaps and slats was calculated using reference 3, page 349, equation 12.37. Table 17 lists the various component skin frictions.

	Wetted Area (sqft)	Form Factor	Flat Plate Area (sqft)	C_{Do}
Wing	73.9	0.99	0.340	0.0096
Verticals	7.22	0.78	0.01	0.0000
Landing gear	0.08	2.00	0.17	0.0012
Engines	0.08		0.08	0.0020
Flaps				0.0044
Slats				0.0044
Total				0.0216

Table 17 – Component Skin Friction Values

The other part of the drag equation is induced drag, which is given by:

$$C_{di} = C_L^2 / \pi ARe \quad (19)$$

Where:

$$e = 1.78*(1-0.045*AR\ ^{0.68})-0.64 = 0.91 \text{ (reference 3, page 361)} \quad (20)$$

$$e_{low\ speed} = 0.9e = 0.9*0.91 = 0.82 \quad (21)$$

An Excel spreadsheet was utilized to sum the drag, then the low speed L/D vs. C_L and C_D vs. C_L^2 polars were created in Figures 18 and 19. From Figures 18 and 15, the drag vs. available thrust was calculated to be 19 : 9.4 or roughly 2:1. Thus the aircraft has adequate thrust margin at takeoff to avoid mushing back into the runway at high AOA's.

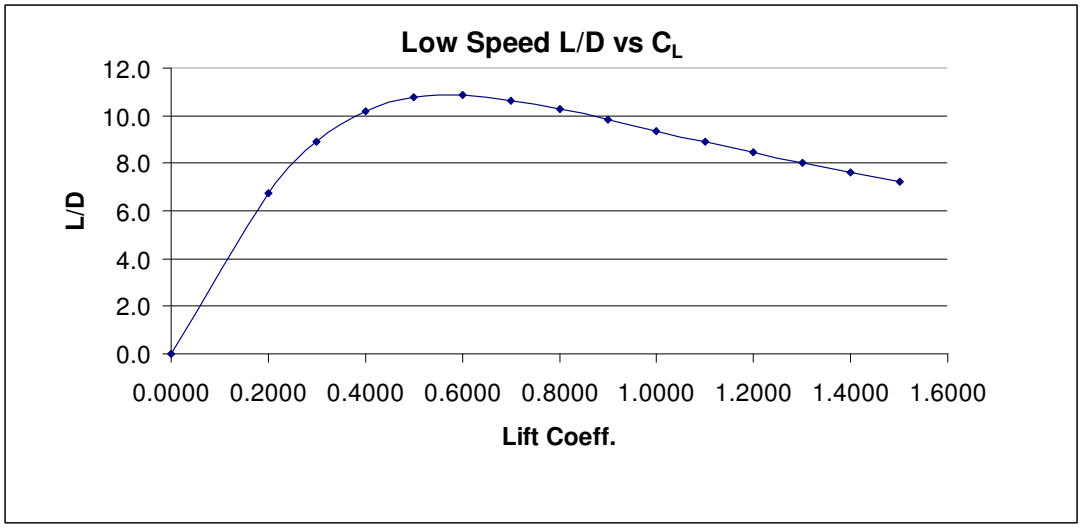

Figure 18 – Low Speed L/D vs. C_L

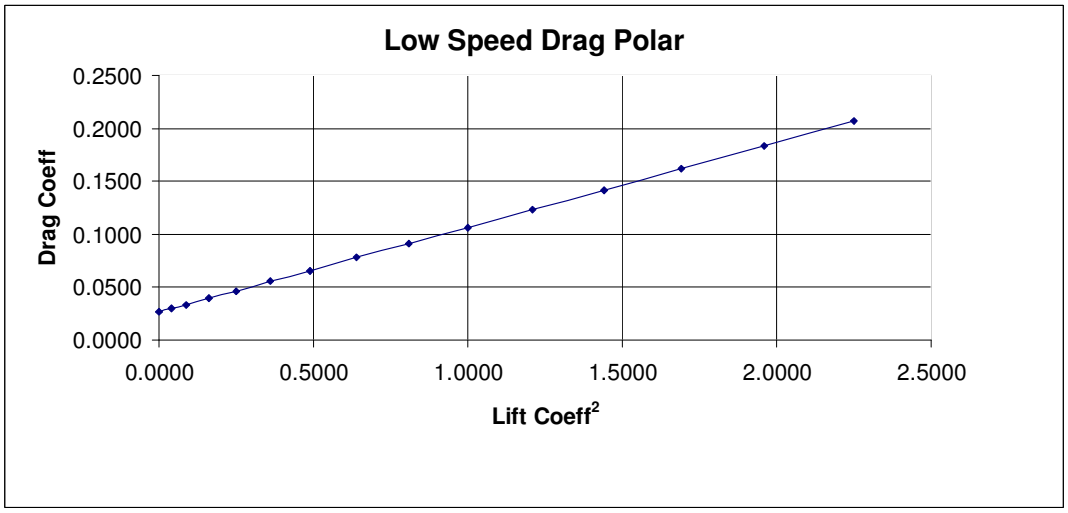

Figure 19 – Low Speed Drag Polar

Takeoff velocity was calculated using equation (22):

$$Vto = [2W/(Sref\ \rho\ .8\ C_{Lmax})]^{0.5} = 23\ kts \qquad (22)$$

Where:
W = 55 lbs
Sref = 5300 sqin
C_{Lmax} = 1.06
ρ = .00238 psf

The aircraft has a zero degree ground incidence to minimize ground roll drag, giving at ground roll $C_D = 0.025$ (Figure 19) and a ground roll drag force of 1.3 lbs. Using Figures 19 and 15, the mean takeoff acceleration at 0.7Vto, 16.1 kts, was calculated by the following equation (reference 2, page 9):

$$a @ 0.7Vto = (g/w)[T - D - Fc(W - L)] = 10.13 \text{ ft/sec}^2 \quad (23)$$

Where:
g = 32.2 ft/sec^2
Fc = rolling friction coeff = 0.03
T = 20 lbs (Figure 15, $C_L = 0.7$)
D = 1.3 lbs
W-L = 55-8.5 = 46.5 lbs

Finally, the Sg, or ground roll distance, was calculated per equation (24) (reference 2, page 10)

$$S_G = V_{to}^2 / (2a_{mean}) = 74 \text{ feet} \quad (24)$$

This is within the required 100-foot takeoff distance.

X. Fabrication

The build took place at the team captain's home in Long Beach. Each part template was printed from CAD for accuracy and speed of fabrication. The center section ribs were balsa with foam core sandwich for strength. The spars were spruce and the shear webs were 1/8-inch balsa sheet. All hard attach points such as the gear floors, payload bay floors and outer wing attach joints were 1/8 inch plywood / foam sandwich structure. First the center section was jigged by taping VHS cassettes to a table, then sliding the ribs in between the cassettes. The spars were spliced using a coping saw and protractor to get accurate fit. They were then bonded in place using epoxy.

The outer wings were initially going to be made from foam, but the weight penalty was at least 2 lbs. The team then went with standard built up spruce spar caps and balsa shear webs with balsa ribs for the outer wings. This resulted in a very light and strong structure similar to the center section. The fixed slats were cut from a CNC foam machine using a CAD model transferred into CNC code.

The gear, motor tubes and wing attach fittings were aluminum. Overall, the project took 3 – ½ months from design freeze to first flight. The cost of materials was roughly $1500. The cost was kept down by a generous donation of a 6-channel radio.

XI. Payload Prediction Chart

In order to calculate an accurate payload prediction chart, the team created a spreadsheet that allowed drag and lift to vary with altitude. The takeoff speed is increased due to reduced density where:

$$C_{lmax} = W / (1/2\rho V^2 * S_{ref})$$

Therefore, the velocity must be increased to produce the same amount of lift. This increases the ground roll on takeoff. Also, the thrust produced by the propeller is reduced in the same way due to reduced density. The power of the engine is also reduced since the mass flow into the engine is reduced due to lower air density. All of these factors were allowed to vary in the spreadsheet in order to determine the payload prediction equation.

XII. Conclusion

The design and build of this flying wing model was very challenging. The team found that no item could be taken for granted since the configuration was so sensitive to changes in CG, planform shape, airfoil section and propulsion integration. Overall, designing and building a tailless aircraft gave us deeper insight into the design compromises that are a part of aircraft design and construction. We look forward to demonstrating our 'unusual' configuration to the rest of our competitors.

XIII. References

1. Donlan, Charles J. (1944) An Interim Report on the Stability and Control of Tailless Airplanes, Langley Aeronautical Laboratory, Langley Field, VA
2. Nicolae, Dr. Leland (2002) Estimating R/C Model Aerodynamics and Performance
3. Raymer, Daniel P. (1999) Aircraft Design, A Conceptual Approach, AIAA, 1801 Alexander Bell Drive, Reston, VA 20191
4. Jozwiak, R., Kubriynski, K (2007) New Slat Concept for Flow Control Over Airfoil, AIAA 2007-1468
5. de Castro, H.V. (2000) The Longitudinal Controls Fixed Static Stability of Tailless Aircraft, Cranfield University, COA Report Number 0018
6. Gierke, Dave (2005) Airplane Engine Guide, Air Age Media Inc., 100 East Ridge, Ridgefield, CT, 06877-4066

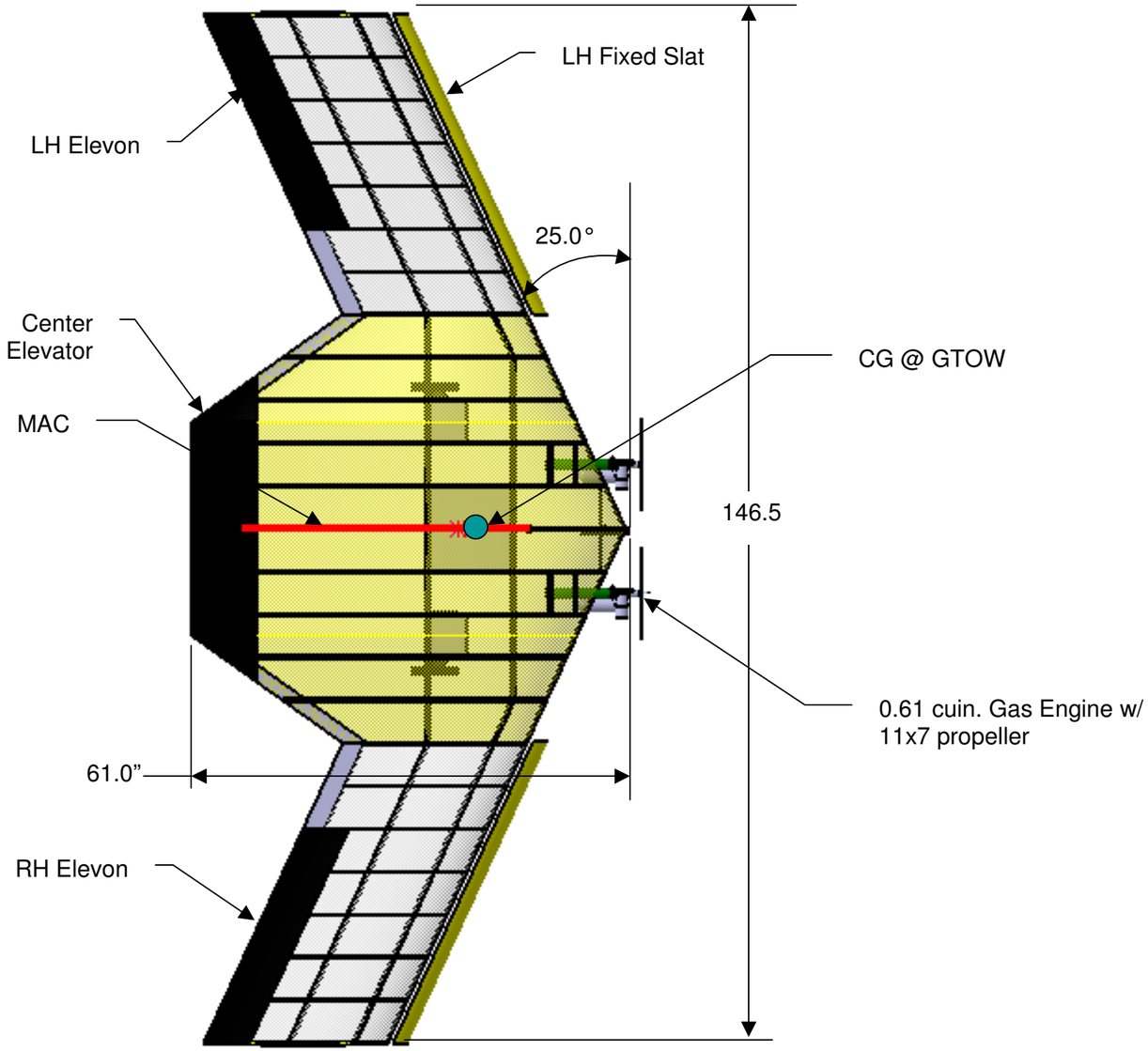

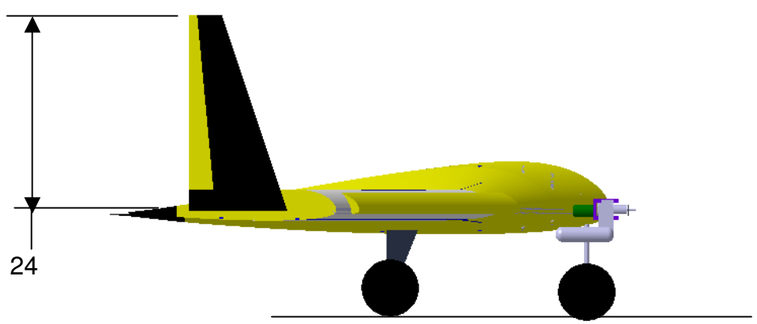

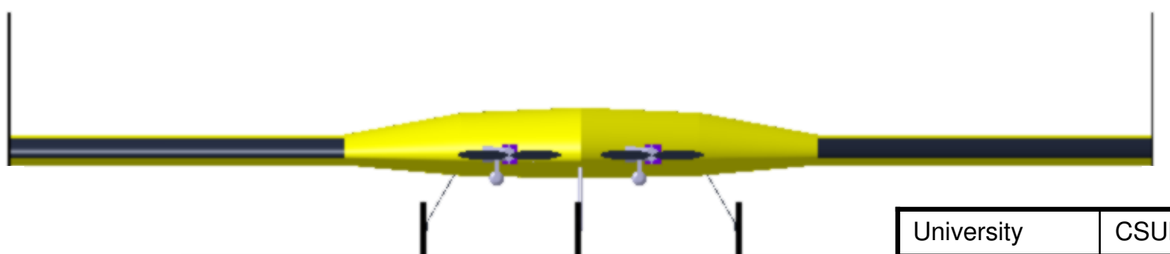

CONFIGURATION DATA	
Sref (sqin)	**5118**
Span (in)	**146.5**
Aspect Ratio	**4.05**
LE Sweep (deg)	**25**
Airfoil t/c (%) & Type	**14.7 / MH78 Modified**
MAC (in)	**40.45**
CG Location at GTOW (in from LE vertex)	**22.05**
Power plant	**2 x 0.61 cuin. Tower Hobbies ABC type Gas**
Propeller	**2 x 11x7 APC**
Weight Empty	**25 lbs**
GTOW	**55 lbs**

University	CSULB
Team Name	A Tailless Tale
Team Number	218

PAYLOAD PREDICTION GRAPH